THE ASTRONOMICAL JOURNAL, 121:362–370, 2001 January

THE NEAR-INFRARED SPECTRUM OF THE PLANETARY NEBULA IC 5117

RICHARD J. RUDY,[1] DAVID K. LYNCH,[1] S. MAZUK,[1] R. C. PUETTER,[2] AND DAVID S. P. DEARBORN[3]

Received 2000 June 15; accepted 2000 September 26

ABSTRACT

Infrared spectroscopy from 0.8 to 2.5 μm is presented for the planetary nebula IC 5117. The emission lines of IC 5117 span a wide range of ionization that includes He II, [S III], [S II], [N I], and H_2. The reddening measured from the hydrogen lines is $E(B-V) = 0.79$, most of which is probably interstellar in origin. The He/H abundance ratio is 0.113 ± 0.015, with approximately 10% of the helium being doubly ionized. Using our measurements of [S II] and [S III] lines and published observations of [S IV], we find a sulfur abundance, relative to hydrogen, of $N(S)/N(H) = 7.8 \times 10^{-6}$, or approximately half the solar value. Fluxes and flux limits for several lines of molecular hydrogen are presented. Measurements of 1–0 transitions, together with the limits on 2–1 transitions, indicate $T_{vib} \sim T_{rot} = 1900$ K, suggesting a purely collisional excitation mechanism. The ortho-to-para ratio is ~ 3, a value that is also indicative of collisional excitation. The presence of [C I] $\lambda 9850$ is consistent with previous studies of IC 5117 that indicated carbon is more abundant than oxygen. IC 5117 follows the trend of planetary nebulae that display bipolar outflows and H_2 emission to be carbon-rich. We confirm the results of Zhang & Kwok, who reported infrared continuum emission substantially in excess of that produced by the ionized gas. This emission is most likely due to hot dust ($T \sim 1300$ K) and accounts for roughly half of the continuum between 1.5 and 2 μm.

Key words: infrared radiation — planetary nebulae: individual (IC 5117)

1. INTRODUCTION

In the last decade, the implementation of modern infrared detector arrays in astronomical spectrographs has resulted in a surge of near-infrared observations of planetary nebulae (PNe) (see Hora, Latter, & Deutsch 1999 and references therein). There are several reasons why spectroscopy of PNe in this wavelength regime is of interest: (1) There are a wealth of atomic lines that reveal the properties of the emission-line gas. These lines both complement and supplement the ultraviolet and optical features. (2) The most observable lines of molecular hydrogen lie in this wavelength range. These provide diagnostics of the neutral/molecular gas that can dominate the mass of the nebula in some young PNe. (3) The near-infrared presents a particularly advantageous region to study the continuum emission from the ionized nebula. The continuum of the exciting star, which frequently dominates the ultraviolet and may contribute significantly to the optical, is falling rapidly in the near-infrared while the emission from warm dust, which contributes the bulk of the radiation in the thermal infrared, is only beginning to rise. The presence of this "notch" makes the near-infrared the best region in which to observe the continuum emission from the ionized gas of the nebula.

In this paper, we present spectroscopy of IC 5117, a compact planetary nebula with numerous atomic lines, molecular hydrogen emission (Isaacman 1984), and peculiar continuum emission around 1.6 μm (Zhang & Kwok 1992, hereafter ZK). The atomic and ionic emission lines are used to derive the reddening and properties of the ionized gas. Detections and limits of a number of H_2 features are used to investigate the molecular gas, and the continuum emission of the nebula is considered with regard to our broad wavelength coverage.

2. OBSERVATIONS

The infrared spectrophotometry of IC 5117 was acquired on the night of 1999 August 30 (UT) with the 3 m Shane reflector of Lick Observatory. The instrument used was the Aerospace Near-Infrared Imaging Spectrograph, which is described in more detail by Rudy, Puetter, & Mazuk (1998). Briefly, the spectrograph uses two channels, each containing a collimator, grating, camera, and detector array, to provide nearly continuous coverage between 0.8 and 2.5 μm. A beam splitter that switches from reflection to transmission at 1.38 μm separates the channels. The detectors are two-quadrant NICMOS3 devices providing 256 channels in the spectral dimension and 128 in the spatial. The spatial resolution is 1″ pixel^{-1}. A 600 line mm^{-1} grating blazed at 1.0 μm operates in the "blue" channel while a 300 line mm^{-1} blazed at 2.0 μm services the red. Each channel has a nearly constant resolution, 16 Å for the blue channel and 37 Å for the red, when using the 3″ slit width employed for our observations of IC 5117. In the spatial dimension, light from a 6″ interval centered on the nucleus was combined to form the spectrum. This was to account for variations in the seeing and guiding and to encompass emission beyond the nominal 1.″4 optical diameter of the nebula (Aaquist & Kwok 1991).

The data were acquired by placing IC 5117 at two positions separated by 34″ (positions A and B) along the east-west–oriented slit and switching between them in the standard ABBA sequence. Individual measurements were 10 s long, an integration time set so that the brightest emission lines would not saturate. Each channel of the spectrograph has 24 mm of free spectral range, but the detectors are only 1 cm in size. To provide full spectral coverage, the detectors are translated between three widely separated but

[1] Space Science Applications Laboratory, M2-266, The Aerospace Corporation, Los Angeles, CA 90009-2957; richard.j.rudy@aero.org, david.k.lynch@aero.org, steve.mazuk@aero.org.

[2] Center for Astrophysics and Space Sciences, C-0111, University of California, San Diego, 9500 Gilman Drive, La Jolla, CA 92093-0424; rpuetter@ucsd.edu.

[3] Lawrence Livermore National Laboratory, P.O. Box 808, Livermore, CA 94551; dearborn2@llnl.gov.

overlapping positions. Two observations, separated by 2.5 pixels, are acquired at each of these locations to provide oversampling and correction for bad pixels.

To remove the instrumental response and reduce the effects of atmospheric absorption, the data were reduced by dividing the raw spectrum of IC 5117 by that of the comparison star HR 8291, an A2 V with $V = 6.11$ mag. It was observed immediately after IC 5117 using the same slit width and orientation. To remove its intrinsic spectrum from this ratio, a model from Kurucz (1991) approximating this spectral type was used. A division of the standard by the model showed that the hydrogen lines, which are prominent in absorption for stars of this spectral class, were not entirely absent from the ratio. To correct for this, the model was smoothed until the line widths matched those of the standard (the equivalent widths of the model matched well with those of the standard, and no modifications were required). An absolute flux scale was set by normalizing to the K magnitude for HR 314 of 5.98. The K magnitude was calculated from the V magnitude tabulated in the Bright Star Catalogue (Hoffleit & Jaschek 1982) and the nominal $V-K$ color for an A2 dwarf from Koornneef (1983). The spectra of IC 5117 resulting from this process are shown in Figures 1 and 2.

Identifications, wavelengths, fluxes, and flux errors for the emission lines of IC 5117 are presented in Table 1. Line fluxes were measured both by fitting Gaussians to, and by computing the "area" of, the individual features. Errors in the *relative* line strengths are estimated by comparing multiple scans and then adjusting the values for factors such as blending with other features, transparency of the atmosphere, and uncertainties in the levels of the nearby continuum. Uncertainties in the *absolute* flux level, as gauged from repeated observations of many of our program sources, are typically less than 20%. In the case of IC 5117, however, the agreement with previous studies is better than this value. ZK covered the region from 1.5 to 1.75 μm (H band) and reported a level for the continuum of 4.4×10^{-18} W cm^{-2} μm^{-1}; our value in the same units is 4.6×10^{-18}. For Br10, the feature to which ZK normalized the remainder of their line fluxes, they measured a flux of $(4.0 \pm 0.4) \times 10^{-13}$ ergs cm^{-2} s^{-1}; our value is 4.1×10^{-13}. Geballe, Burton, & Isaacman (1991) observed IC 5117 in the 2–2.4 μm range. The level of the K-band continuum in their spectrum is 6.0×10^{-18} W cm^{-2} μm^{-1}; our level in the same spectral range is 5.6. Moreover, our Brγ flux of 12.2×10^{-13} ergs cm^{-2} s^{-1} is virtually identical to their value of 12.1×10^{-13}.

Blended features were deconvolved by using a least-squares procedure that assumed Gaussian profiles of identical widths for each of the components. That line width, plus the central wavelengths and amplitudes of the individual

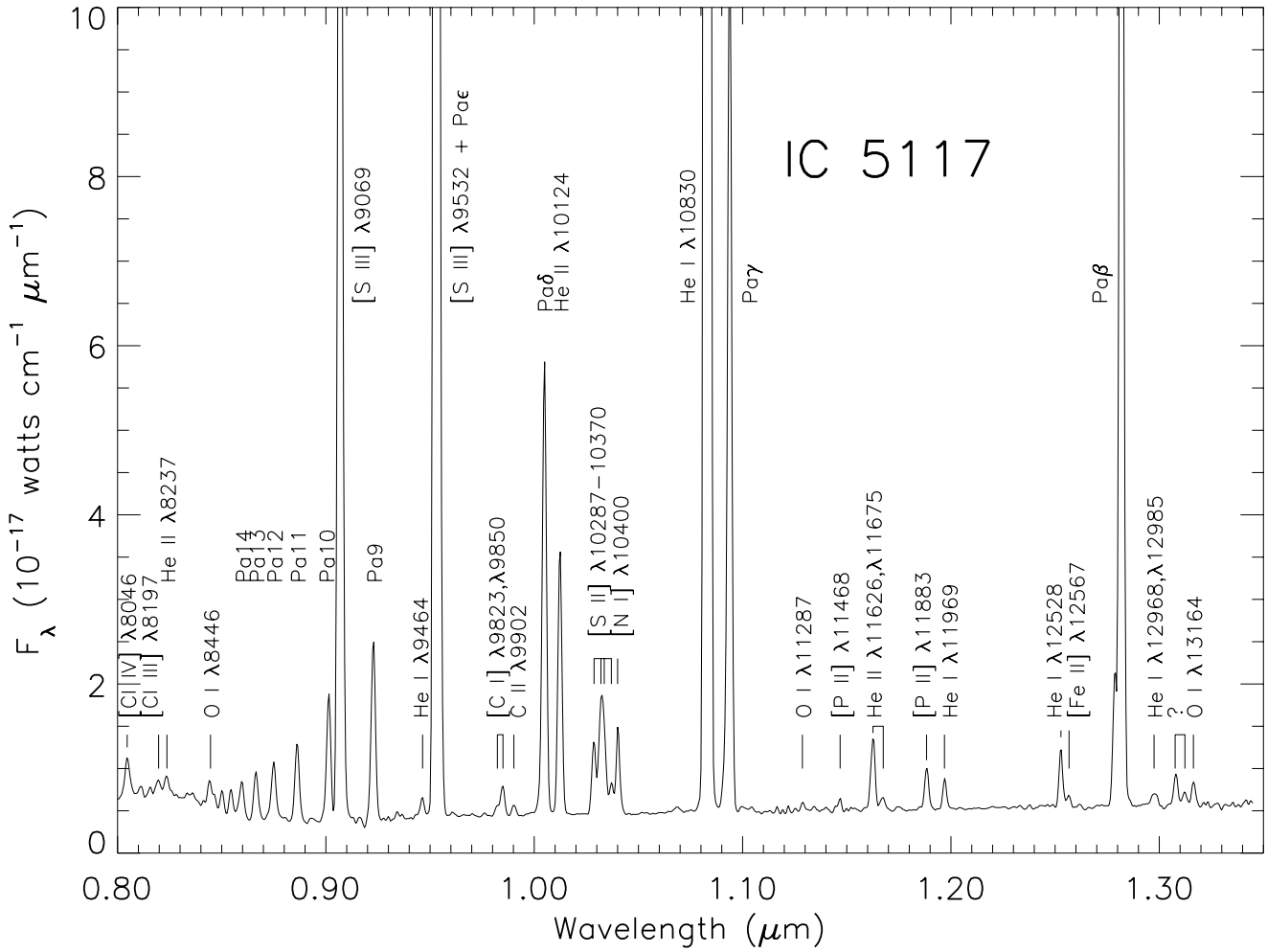

FIG. 1.—Spectrum of IC 5117 from 0.8 to 1.35 μm with identifications for the emission lines. The scale on the ordinate is set to show the weaker lines and the continuum.

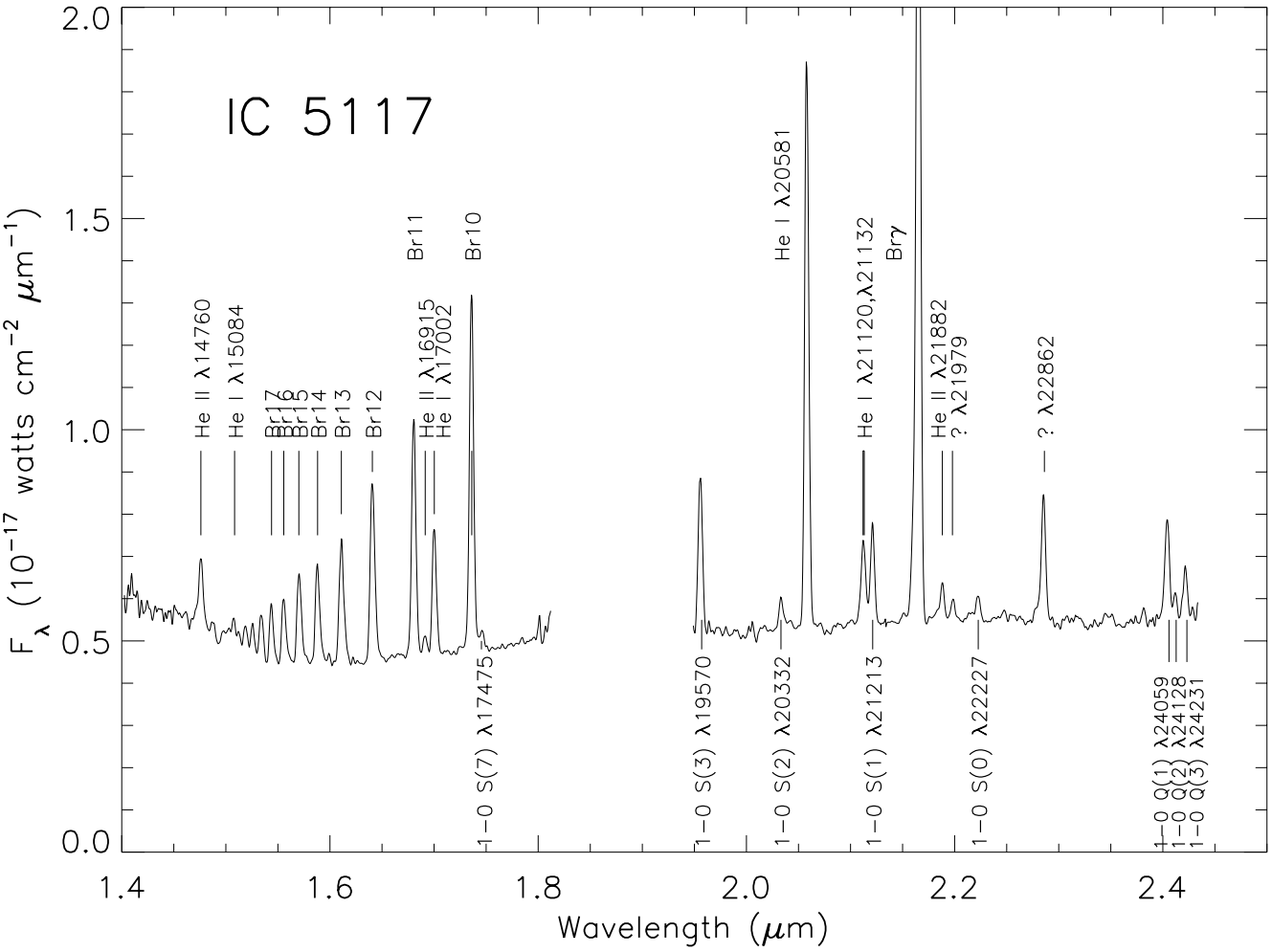

FIG. 2.—Spectrum of IC 5117 from 1.4 to 2.45 μm with identifications for the emission lines. The gap in the data at 1.9 μm is due to atmospheric absorption.

components, was determined by the fitting procedure, and the wavelengths checked for agreement with the laboratory values. Blended lines that were deconvolved in this manner included O I λ8446 and Pa16, [C I] λ9823 and λ9850, the complex of [S II] lines (λ10287, $\lambda\lambda$10320, 10336, λ10370) and [N I] λ10400, He I λ12528 and [Fe II] λ12567, He I $\lambda\lambda$12785, 12790 and Paβ, unidentified features λ13076, λ13123 and O I λ13164, Br10 and H_2 1–0 $S(7)$ λ17475, and the three H_2 lines λ24059, λ24128, and λ24231.

3. RESULTS AND DISCUSSION

IC 5117 is a distant object (Phillips 1998) that lies very close to the Galactic plane ($b = -5.^\circ1$). As such, it is expected to be significantly reddened, and in fact, that has been confirmed by previous studies. Because the reddening must be accounted for in the analysis of the emission lines and the continuum, we begin this section with a determination based on our observations.

3.1. *Hydrogen Lines and Reddening*

The reddening of IC 5117 is measured by comparing the observed ratios of the hydrogen lines (to Paβ) with their case B values and assuming that the extinction properties of the dust are described by the reddening curve of Draine (1989). The case B values are from the calculations of Storey & Hummer (1995) for an electron temperature and density of 1.1×10^4 K and 3.6×10^4 cm^{-3}, respectively. The electron temperature is an average of values derived from the [O III] and [N II] lines (McKenna et al. 1996), while the density is taken from the compilation of Stanghellini & Kaler (1989). We will use these values throughout the remainder of the paper.

The reddening is obtained from a least-squares fit to a plot of the observed line ratios divided by the case B values as a function of extinction at the wavelength of the respective line (see Fig. 3). Eight Paschen lines and six Brackett lines were used in the fit. The best-fit value is $E(B-V) = 0.79 \pm 0.08$, where the error reflects both the scatter in the data points and uncertainties in the temperature and density. This is marginally smaller than the value of $E(B-V) = 0.88$ found by ZK using the radio continuum–to–Hβ ratio, the depth of the 2200 Å feature, and the Balmer decrement. This was also the value reported by Aller & Czyzak (1983) from analysis of their earlier observations (Aller & Czyzak 1979).

The reddening through the Milky Way in the direction of IC 5117 derived from the *COBE/IRAS* maps of Schlegel, Finkbeiner, & Davis (1998) is $E(B-V) = 0.77$. Although this is comparable to the value we measure, IC 5117 is thought to be 10 kpc distant (Phillips 1998) and thus should not experience the full reddening of the Galactic plane.

TABLE 1

OBSERVED EMISSION-LINE STRENGTHS OF IC 5117

Identification	Wavelength[a] (Å)	$F/F(\mathrm{Pa}\beta)$	Identification	Wavelength[a] (Å)	$F/F(\mathrm{Pa}\beta)$
[Cl IV]	8046	0.027 ± 0.005	Paβ	12818	1.000
?	8109	0.009 ± 0.004	He I	12968, 12985	0.010 ± 0.0025
?	8158	0.005 ± 0.004	?	13076	0.018 ± 0.004
[Cl III]	8197	0.012 ± 0.004	?	13123	0.008 ± 0.004
He II 9–5	8237	0.015 ± 0.004	O I	13164	0.016 ± 0.004
O I	8446	0.015 ± 0.004	He II 9–6	14760	0.015 ± 0.004
Pa16	8502	0.009 ± 0.004	He I	15084	0.004 ± 0.002
Pa15	8545	0.012 ± 0.004	Br20	15192	0.005 ± 0.004
Pa14	8598	0.021 ± 0.004	Br19	15261	0.005 ± 0.004
Pa13	8665	0.029 ± 0.004	Br18	15342	0.010 ± 0.003
Pa12	8750	0.039 ± 0.004	Br17	15439	0.013 ± 0.003
Pa11	8863	0.049 ± 0.005	Br16	15556	0.016 ± 0.003
Pa10	9015	0.072 ± 0.006	Br15	15701	0.019 ± 0.003
[S III]	9069	0.973 ± 0.05	Br14	15881	0.023 ± 0.003
Pa9 + ?	9229	0.106 ± 0.01	Br13	16109	0.031 ± 0.003
He I	9464	0.008 ± 0.003	Br12	16407	0.046 ± 0.003
[S III] + Pa8	9532, 9545	3.14 ± 0.15	Br11	16806	0.055 ± 0.003
[C I]	9823	0.0024 ± 0.0008	He II 12–7	16915	0.004 ± 0.001
	9850	0.016 ± 0.0008	He I	17002	0.029 ± 0.02
C II	9902	0.005 ± 0.002	Br10	17362	0.083 ± 0.008
Paδ	10049	0.237 ± 0.01	H_2 1–0 $S(7)$	17475	0.0044 ± 0.0012
He II 5–4	10124	0.152 ± 0.08	Br9	18174	Atmosphere
[S II]	10287	0.040 ± 0.004	Br8	19446	Atmosphere
	10320, 10336	0.097 ± 0.006	H_2 1–0 $S(3)$	19570	0.035 ± 0.01
	10370	0.017 ± 0.004	H_2 1–0 $S(2)$	20332	0.0074 ± 0.002
[N I]	10400	0.044 ± 0.004	?	20415	0.002 ± 0.001
He I	10830	7.54 ± 0.37	He I	20581	0.130 ± 0.02
Paγ	10938	0.486 ± 0.025		21120, 21132	0.021 ± 0.002
O I	11287	0.004 ± 0.0015	H_2 1–0 $S(1)$	21213	0.023 ± 0.002
[P II]	11468	0.004 ± 0.0012	Brγ	21655	0.248 ± 0.012
He II 7–5	11626	0.042 ± 0.003	He II 10–7	21882	0.007 ± 0.001
He II 11–6	11673	0.008 ± 0.002	?	21985	0.004 ± 0.001
[P II]	11883	0.022 ± 0.0015	H_2 1–0 $S(0)$	22227	0.005 ± 0.001
He I	11969	0.016 ± 0.0015	?	22862	0.030 ± 0.003
	12528	0.029 ± 0.0015	H_2 1–0 $Q(1)$	24059	0.025 ± 0.0015
[Fe II]	12567	0.006 ± 0.0015	H_2 1–0 $Q(2)$	24128	0.005 ± 0.0015
He I	12785, 12790	0.073 ± 0.02	H_2 1–0 $Q(3)$	24231	0.011 ± 0.0015

NOTE.—$F(\mathrm{Pa}\beta) = 4.95 \times 10^{-12}$ ergs cm^{-2} s^{-1}.

[a] Laboratory wavelengths as measured in air.

However, the distance is sufficient to account for much of the extinction we measure. Thus, despite the considerable thermal infrared emission from IC 5117 that is attributable to warm dust (Volk & Cohen 1990), most of the reddening is probably interstellar, rather than intrinsic, in origin.

3.2. He I *and* He II *lines and the Helium Abundance*

The He II λ10124 5–4 transition is the strongest He II transition in the infrared. It is present in IC 5117 at sufficient strength to indicate that He^{++} constitutes a non-negligible fraction of the helium in the nebula. To compute its abundance, we take the observed line strengths relative to Paβ, correct these for the reddening found from the hydrogen lines, and compare them with the case B values (again taken from Storey & Hummer 1995). This yields an abundance of $He^{++}/H^{+} = 0.012 \pm 0.0011$. These results are illustrated in Figure 4, which displays the scatter of the abundance determined from each of the individual lines about the average value.

Finding the abundance of He^{+} (via the He I lines) is more difficult, primarily as a result of the metastability of the $2\,^3S$ level. As in many PNe, the λ12528/λ11969 value of 1.7 is significantly greater than the recombination value of 0.66 (Rudy et al. 1993). This is due to self-absorption of He I λ3188, which has $2\,^3S$ as its lower level. The subsequent branching from its upper level, $4\,^3P$, then enhances λ12528 (Lowe, Moorhead, & Wehlau 1979). Because λ12528 is not given by the recombination value, it was not used in calculating the He^{+} abundance. The lines that were used are shown in Figure 4 and listed in the accompanying legend; their recombination values are taken from the calculations of Smits (1991). The result is $He^{+}/H^{+} = 0.101 \pm 0.014$. Combining this with the $He^{++}/H^{+} = 0.012$ yields an H/He value of 0.113 ± 0.015, in good agreement with the value of 0.11 reported by Aller & Czyzak (1983).

3.3. [S II] *and* [S III] *Lines and the Sulfur Abundance*

Forbidden lines are used to determine the abundances of the heavy elements in emission-line nebulae, and unfortunately, few elements display prominent forbidden lines in the near-infrared. A notable exception is sulfur, which has multiple lines from two different ionization states. These are

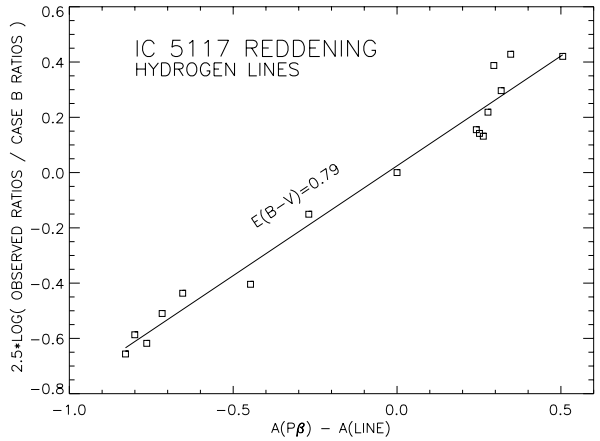

FIG. 3.—Reddening of IC 5117 as derived from the hydrogen lines. In this plot the abscissa is the differential extinction, in units of $E(B-V)$, between Paβ and the other hydrogen lines. The ordinate is the observed flux ratio of a given line to Paβ divided by the case B value for the same ratio. With this choice of axes, the reddening value is equal to the slope of a linear fit to the data points. For IC 5117, this is $E(B-V) = 0.79$. Given the low Galactic latitude of IC 5117 ($b = -5.^{\circ}1$), most of the extinction is likely to be interstellar in origin.

[S II] λ10287, $\lambda\lambda$10320, 10336, and λ10370 and [S III] λ9069 and λ9532. These features are useful for determining the sulfur abundance for a number of reasons: (1) They are strong and fall in regions of good atmospheric transmission. (2) They are less sensitive to uncertainties in the reddening than their ultraviolet and optical counterparts. (3) Their critical densities are sufficiently large ($\sim 10^6$ cm^{-3}) that they do not suffer significant collisional de-excitation in most PNe. For the electron temperature and density, we use our adopted values of 11,000 K and 36,000 cm^{-3}, respectively.

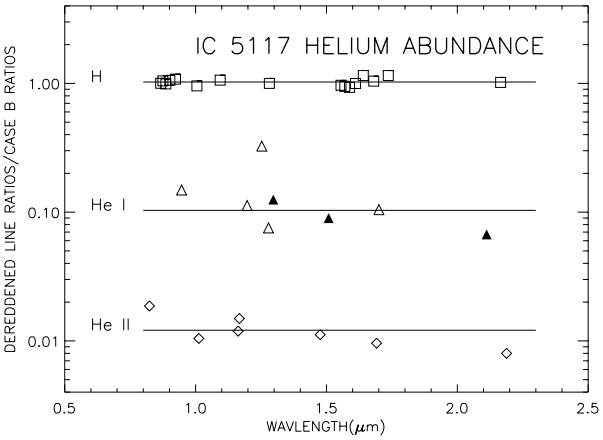

FIG. 4.—Helium-to-hydrogen abundance for IC 5117. The ordinate is the reddening-corrected flux ratio of the H, He I, or He II line, with respect to Paβ, divided by the case B value for the same ratio. Hydrogen lines are plotted as squares, He I as triangles (open for singlets, filled for triplets), and He II as diamonds. The individual lines can be identified from their wavelengths; for He I they are λ9464, λ11969, λ12785, $\lambda\lambda$12968, 12985, λ17002, and $\lambda\lambda$21120, 21132 ($\lambda\lambda$12968 and 12985 have been combined, as have $\lambda\lambda$21120 and 21132). He I λ12528 is shown in the figure but was not used in the abundance determination, because of its well-known enhancement due to optical depth effects in λ3188 (see text). The He II lines are λ8237, λ10124, λ11626, λ11673, λ14760, λ16915, and λ21882. In this presentation, the relative abundance indicated by each line for its parent species can be read off of the y-axis. The horizontal lines indicate the average value for each of the species. The average relative abundances, by number, are $H^+/He^+/He^{++} = 1.00/0.101/0.012$.

The S^+ abundance is computed using a standard five-level atom and the transition probabilities tabulated by Mendoza (1983) and collisional strengths calculated by Keenan et al. (1996). The result is $N(S^+)/N(H^+) = (3.7 \pm 1.0) \times 10^{-7}$. Using the same electron density and temperature, and the collision strengths of Galavís, Mendoza, & Zeippen (1995), a similar calculation for S^{++} gives $N(S^{++})/N(H^+) = (2.8 \pm 0.4) \times 10^{-6}$. The flux in the [S IV] fine-structure line at 10.5 μm is 2.0×10^{-11} ergs cm^{-2} s^{-1} (Gillett, Merrill, & Stein 1972; Beck et al. 1981). It strength implies a relative abundance of $N(S^{+3})/N(H^+) = (3.2 \pm 0.8) \times 10^{-6}$, indicating that the majority of the sulfur is triply ionized. The sum of the three ionization states is 6.4×10^{-6}; multiplying by the ionization correction factor of 1.18 (Aller & Czyzak 1983) yields, for the total sulfur abundance, 7.5×10^{-6}. For comparison, Aller & Czyzak (1983) found 10.5×10^{-6}, using $E(B-V) = 0.88$, different lines, and older values for the collisional rates. Note that our value is only about 40% of the solar value (Grevesse & Anders 1989; Grevesse, Noels, & Sauval 1996).

3.4. [P II] *and the Phosphorous Abundance*

IC 5117 is one of the minority of PNe that display the near-infrared forbidden lines of [P II]. The strongest of these, λ11883, was first detected by Treffers et al. (1976) in NGC 7027; Rudy et al. (1992) later observed the weaker companion feature λ11468 in the same object. Hora et al. (1999), in their extensive infrared spectroscopic survey of PNe, detected a feature at $\sim$1.1892 μm (vacuum wavelength) in about a third of the objects they observed. They do not present a positive identification for this line, but we believe that in most of these objects it is [P II] λ11883. This is because the group includes NGC 6572, BD $+30^{\circ}3639$, and NGC 7027, nebulae in which the identification of [P II] λ11883 has been confirmed by the detection of [P II] λ11468 (Rudy et al. 1991b, 1991a, 1992).

The determination of the phosphorous abundance is difficult because lines from ionization states other than the first generally lie in spectral regions that are inaccessible. However, a crude estimate can be made by a comparison with sulfur since the first five ionization levels are similar for the two elements, and because lines from multiple ionization states of sulfur are observable (see § 3.3). Following the procedure of Rudy et al. (1991b), we find, from [P II] λ11883, $N(P^+)/N(H^+) = 2.0 \times 10^{-8}$. Then, by assuming $N(P^+)/N(P_{tot}) = N(S^+)/N(S_{tot})$, a total phosphorous abundance of $(4.1 \pm 2) \times 10^{-7}$ relative to hydrogen is calculated. The large errors result from the uncertainty in the atomic parameters, the sensitivity of the λ11883 intensity to electron temperature, and the fact that only a small fraction of the phosphorous is singly ionized. The nominal abundance derived is slightly greater than both the solar (2.8×10^{-7}) and meteoritic (3.3×10^{-7}) values (Grevesse & Anders 1989; Grevesse et al. 1996), but the large uncertainties allow for a value below solar as well.

Despite the uncertainty in the phosphorus abundance, it is clear the original formation site for the heavy elements of IC 5117 was a Type II supernova. The much lower abundance of the odd elements (e.g., phosphorus) relative to even elements (e.g., sulfur) is quite distinctive and a clear signature of the nucleosynthesis that occurs in the supernova explosions of massive stars (Hoffman et al. 1999). Since phosphorus is more than an order of magnitude less abun-

dant in IC 5117 than sulfur, the phosphorous-to-sulfur abundance ratio was not altered substantially in the IC 5117 progenitor.

To investigate whether the $N(P)/N(S)$ could have been modified *slightly* during the red giant phase of the progenitor, we considered nucleosynthesis through *s*-process neutron capture, a process that is known to occur in many red giants. Solutions of the equations for neutron capture were obtained using the cross sections of Woosley et al. (1978). The results indicated that phosphorous is rapidly enhanced with respect to sulfur shortly after the onset of neutron capture. This is not surprising, since phosphorous is much less abundant than its lower neighbor in the nuclear sequence (silicon), which is converted to phosphorous as it captures neutrons. Sulfur is not similarly increased, since it is produced from phosphorous, which is initially scarce. Thus a small amount of *s*-processing can readily produce an enhanced $N(P)/N(S)$ value. To see whether this is likely to have occurred for IC 5117, we extended the calculations to include chlorine, which is the next odd-numbered element in the nuclear sequence. The chlorine abundance was found to rise initially at an even greater rate than phosphorous. Therefore, if phosphorous were enriched in IC 5117, an even greater enhancement of chlorine would be expected. This is not what is observed. Aller & Czyzak (1983) report a chlorine abundance of 1.4×10^{-7}, yielding an $N(Cl)/N(S)$ value that is very nearly solar. Thus, it is probable that the $N(P)/N(S)$ value in IC 5117 is close to the solar ratio as well.

3.5. [C I]

Neutral carbon is readily ionized, so the existence of [C I] features requires an environment sheltered from the ionizing radiation. Moreover, it requires that the abundance of carbon exceed that of oxygen, since formation of CO will deplete the scarcer of the two elements. The presence of [C I] λ9823 and λ9850 underscores the carbon-rich $[N(C) > N(O)]$ nature of IC 5117 known from previous optical studies [e.g., Aller & Czyzak 1983 give $N(C)/N(O) \sim 2$], and the carbon-rich nature of its circumstellar dust grains (Volk & Cohen 1990). Thus IC 5117 follows the trend of carbon-rich PNe to be associated with bipolar outflows (Zuckerman & Aller 1986) and molecular hydrogen emission (Kastner et al. 1996; see § 3.7).

3.6. *Other Atomic and Ionic Emission Lines*

There are a number of other emission lines in the spectrum of IC 5117 that merit comment. Three are permitted lines of neutral oxygen: λ8446, λ11287, and λ13164. The O I lines in PNe are produced by recombination, continuum fluorescence, and fluorescence by Lyβ. These processes are discussed by Bowen (1947), Grandi (1975, 1976, 1980), and Rudy, Rossano, & Puetter (1989). The Lyβ fluorescence mechanism produces λ8446 and λ11287 photons in equal numbers and is the dominant process when these two lines are very strong. The presence of O I λ13164 > λ11287 in IC 5117, however, indicates that fluorescence by the stellar continuum is the principal creation mechanism in this planetary nebula.

ZK reported the detection of Mg I at 1.5047 μm and three weak features of Si I that are not seen in our data. The nearest line feature to the wavelength of the Mg I line is He I λ15084, which is not identified by ZK but is present in our data at a strength commensurate with the other He I features. With regard to the Si I lines and two unidentified features lying between Br11 and Br12 that also are missing from our spectrum, we can only note that other emission lines of comparable equivalent width are detected in our data. If the features are spurious, a possible way that they could be introduced is through division of the spectrum of the source by that of the standard. ZK represented their standard star BS 8252, a G8 III, with a 4500 K blackbody. However, a giant of this spectral type is not featureless in this wavelength region, and weak absorption features (such as the second overtone of CO) will produce apparent weak emission features in the source spectrum upon division. In any case, high-resolution spectrographs now exist that can confirm or rule out the presence of these lines.

We do confirm the presence of the two unidentified lines, at 2.199 and 2.287 μm, observed by Isaacman (1984). These features were first discovered in NGC 7027 by Smith, Larson, & Fink (1981). Their presence in several PNe has been established by Geballe et al. (1991), who discuss the range of ionization energies between which the parent ion is likely to fall.

3.7. *Molecular Hydrogen*

The importance of H_2 in PNe derives in part from the fact that molecular gas may dominate the shell mass for young planetary nebulae (Huggins & Healy 1989). In addition, the numerous lines of H_2 can provide measures of the density, temperature, dust content, and excitation mechanism of the molecular gas, as well as insight into the actual formation process (Schwartz, Cohen, & Williams 1987; Black & van Dishoeck 1987; Tanaka et al. 1989; Martini, Sellgren, & Hora 1997). In fact, the presence of H_2 emission is now a criterion used in the classification of PNe (Hora et al. 1999).

The existence of molecular gas in IC 5117 has been established at radio wavelengths by the detection of H I (Taylor, Gussie, & Pottasch 1990) and CO absorption (Gussie & Taylor 1995; Dayal & Bieging 1996), and from near-infrared spectroscopy (Isaacman 1984; Geballe et al. 1991) and imaging of the 1–0 $S(1)$ line (Kastner et al. 1996).

Because H_2 is formed from two identical particles, its rotational-vibrational spectrum differs from those of most diatomic molecules. It has no permanent dipole moment, so "permitted" transitions do not occur. The molecule can radiate in modes other than as an electric dipole, but the associated transition rates are much lower. In fact, the states are sufficiently long-lived that generally, *within a given vibrational state*, the levels are populated thermally. If the relative line strengths for a few of the transitions can be measured, then this information can be combined with their respective statistical weights to derive the rotation temperature for that vibrational level. If collisions alone excite the molecular hydrogen, then populations in different vibrational states can also be described by this same temperature. However, if the excitation mechanism includes a fluorescence component (which is frequently the case), higher vibrational states will be overpopulated, indicating a temperature different from, and higher than, the rotational value.

Figure 5 provides a graphical determination of the temperature and excitation mechanism of the molecular hydrogen of IC 5117. Emission-line strengths are plotted as a function of excitation energy in the standard manner used for the analysis of H_2 lines (see, e.g., Martini et al. 1997). The temperature can be found directly from the slope of a straight line fitted to the data points, while a comparison of

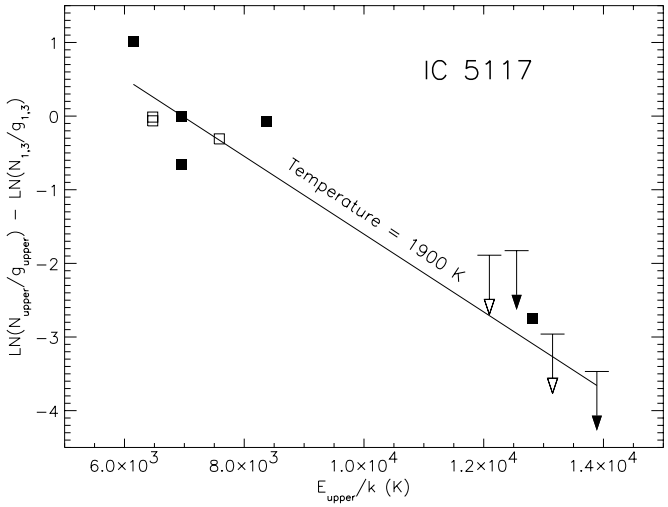

FIG. 5.—Molecular hydrogen rotational and vibrational temperatures for IC 5117. The effective temperature of a specific transition, i.e., the energy of its upper level divided by the Boltzmann constant, is plotted along the abscissa. The ordinate is the natural logarithm of the ratio of the line flux divided by the statistical weight of its upper level to the same quantity for the 1–0 $S(1)$ transition $\lambda 21213$. Open squares denote 1–0 para transitions; filled squares are ortho transitions between the same two vibrational levels. A thermal value for the ortho-to-para ratio has been assumed, that is, ortho:para = 3:1, and this provides a good match to the data. Arrows denote 1 σ limits for 2–1 transitions. Horizontal bars are the 2 σ limits. Again, para transitions are coded as open symbols. The temperature derived from the 1–0 transitions alone (the rotational temperature) is 2200 K and is similar to the value (1900 K) derived using the 1–0 measurements and 2–1 limits. This similarity in temperatures favors a collisional rather than a fluorescent excitation process. See text for additional discussion.

the line ratios can yield insights into the excitation mechanism. Detailed models of the line ratios that characterize the different conditions and excitation mechanisms have been computed by Black & van Dishoeck (1987) and Takayanagi, Sakimoto, & Onda (1987).

To determine the temperature of the molecular hydrogen in IC 5117, two cases were considered. In the first, the fit was only to the 1–0 transitions (i.e., transitions between the first vibrational level and the ground state). In the second, upper limits on the 2–1 transitions were considered as well. The former provides a measure of the rotational temperature, $T_{\rm rot}$, while the latter furnishes an estimate of $T_{\rm vib}$. In the case where collisional excitation dominates, the two temperatures are expected to be similar; in the case where fluorescence contributes strongly to the excitation, $T_{\rm vib}$ should be significantly greater than $T_{\rm rot}$. Our results are $T_{\rm rot} = 2200 \pm 400$ K and $T_{\rm vib} = 1900 \pm 300$ K. While these results are consistent with $T_{\rm vib} \sim T_{\rm rot}$, and a collisional excitation mechanism, it is extremely unlikely that $T_{\rm vib}$ significantly exceeds $T_{\rm rot}$ and that fluorescence plays much of a factor.

One caveat to this interpretation has been raised by Black & van Dishoeck (1987), who noted that at higher densities ($> 10^4$ cm $^{-3}$) collisions can thermalize the lowest-lying vibrational levels, thus mimicking a thermal excitation mechanism. They point out that observations of higher vibrational levels are needed to distinguish unequivocally between collisional and fluorescent excitation processes. The wavelength range spanned by our data encompasses a large number of additional H_2 lines, including several that are observed in sources that are fluorescently excited. Their absence in IC 5117 indicates that ultraviolet fluorescence plays, at most, a minor role in producing the molecular hydrogen emission.

Another aspect of the H_2 observations that supports collisions as the primary excitation mechanism in IC 5117 is the ortho-to-para ratio. Because the H_2 molecule is formed from identical, and thus indistinguishable, nuclei, the exclusion principle comes into play. Since the nuclei are protons with spin $\frac{1}{2}$, the total wave function for the molecule, which is the product of the rotational and spin wave functions, must be antisymmetric. If the spins of nuclei are aligned (ortho state), then the spin wave function is symmetric (even parity) and the rotational wave function must be odd so that their product is odd. Similarly, if the spins of the two nuclei are oppositely directed (para state), the rotational wave function must be even. The symmetry or antisymmetry of the rotational wave function is given by the evenness or oddness of the angular momentum quantum number J. Because the spin state cannot change during a radiative transition, the rotational state must maintain the same evenness or oddness before and after the transition. This accounts for the selection rule $\Delta J = 0, \pm 2$ and why the familiar P- and R-branches are missing from the transitions of H_2. Because there are three spin states of even symmetry and only one of odd, the ortho transitions are 3 times stronger when the ortho-to-para ratio is in statistical equilibrium. While formation of H_2 on dust grains produces a thermal ratio, there are processes that can cause the ortho-to-para ratio to deviate from the thermal value. These are reviewed by Martini et al. (1997), who provide an extensive list of references. Nonthermal ratios can persist in photodissociation regions, and in regions where ultraviolet fluorescence dominates the excitation of H_2, values of 1–1.8 are typical (Tanaka et al. 1989). In addition, Sternberg & Neufeld (1999) have shown that significant optical depths in the transitions can preferentially reduce the line strengths of the ortho transitions, producing line ratios that are less than 3 even though the actual ortho-to-para ratio of the gas is thermal. In IC 5117, however, the measured line ratios are very close to 3, indicating an ortho-to-para ratio that is very close to 3. This result is consistent with statistical equilibrium and a collisional mechanism exciting the H_2 emission.

3.8. *Continuum Emission*

ZK reported excess continuum emission in the 1.5–1.75 μm spectral range. Most of this they attributed to thermal emission from hot dust, but they noted an unexplained steepness to the slope of the continuum. As a possible explanation, ZK suggested the presence of a previously unidentified dust feature. Our much broader wavelength coverage allows us to examine the continuum in detail. Although we see the bulge from the Paschen continuum, there is no indication of any discrete dust emission features. However, there is clearly a large excess to the overall continuum above that expected from the ionized gas. To quantify this, we follow the procedure of ZK and model the data with components from the central star, the hot gas, and the hot dust. To calculate the continuum associated with gas, we use the procedure described by Rudy et al. (1991b). It includes the bound-free, free-free, and two-photon components for H^+, He^+, and He^{++} and normalizes the results to the measured fluxes of the H I, He I, and He II emission lines. The calculations are only weakly dependent on elec-

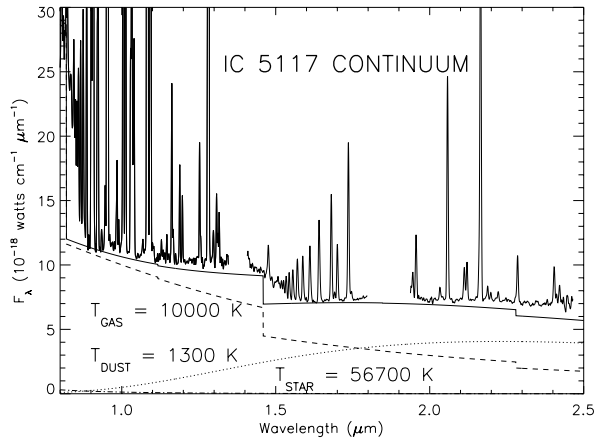

FIG. 6.—Near-infrared continuum emission of IC 5117. The observations, corrected for a reddening of $E(B-V) = 0.79$, are shown together with a model continuum (*heavy line*). The model is the sum of components from three sources: the ionized gas, the central star, and hot dust grains. The former is calculated from the intensities of the H I, He I, and He II emission lines and the electron density and temperature (see text). The temperature and level of the thermal dust emission, and the level of the exciting star, are free parameters and were varied to produce a reasonable fit to the data. The temperature of the star was taken from ZK. What is unusual about the continuum is the magnitude of the contribution from very hot dust—more than half of the flux at 2 μm is from this source, and there is a nonnegligible contribution at 1.2 μm.

tron density (since both the continuum emission and Paschen line fluxes scale almost identically with density) but are sensitive to electron temperature.

The results are shown in Figure 6, where the model for the continuum is plotted together with the reddening-corrected spectrum of IC 5117. The components of the continuum—the gas, the dust, and the central star—are also overplotted. The temperature of the central star (T_{star} = 56,700 K) was taken from ZK, while the temperature of the ionized gas and the extinction are the values discussed above. The only free parameters were the level of the stellar continuum and the temperature and level of the dust emission. The free parameters were set by eye to produce the best fit to the observations.

The model is in good agreement with the observations, and this consistency leads to the following conclusions: (1) The contribution from the central star is very small in the near-infrared. The component shown in Figure 6 represents what is possible rather than what is actually necessary to fit the observations. Because its spectrum follows the Rayleigh-Jeans portion of the blackbody curve ($F_\lambda \sim \lambda^{-4}$), a significant stellar contribution beyond 1 μm would require that it be the dominant contributor at 0.8 μm, which is not seen. (2) A hot dust component ($T_{dust} \sim 1300$ K) is present; the dust emission contributes significantly to the continuum at 2 μm (>50%), and nonnegligibly at 1.2 μm (>10%). It is worthwhile stressing that this is an unusually large portion of the 1–2 μm continuum and is the largest for any planetary nebula of which we are aware. The fact that the model begins to fall below the observations redward of 2 μm is a consequence of considering only a single dust temperature—a more physical model would incorporate a distribution of temperatures. However, the 1300 K component would still remain the hottest of these components and the dominant contributor at the shortest wavelengths.

4. SUMMARY AND CONCLUSIONS

Near-infrared spectroscopy of the compact planetary nebula IC 5117 reveals a rich emission-line spectrum with a broad spread of ionization states ranging from He II on the high end to [C I] and molecular hydrogen on the low. The reddening indicated by the Paschen and Brackett lines is $E(B-V) = 0.79$. The sulfur abundance is about half the solar value. The molecular hydrogen features display relative strengths in concordance with a thermal population and a thermal ortho-to-para ratio, indicating a collisional excitation mechanism. IC 5117 displays one of the largest excesses of emission in the 1–2 μm region that we have encountered and must have substantial amounts of very hot dust.

We are grateful to K. Baker and W. Earthman, the telescope operators at Lick Observatory during these measurements, for their help in acquiring the data. This work was supported by the Independent Research and Development program at the Aerospace Corporation. R. C. P. acknowledges support from NASA.

REFERENCES

Aaquist, O. B., & Kwok, S. 1991, ApJ, 378, 599
Aller, L. H., & Czyzak, S. J. 1979, Ap&SS, 62, 397
———. 1983, ApJS, 51, 211
Beck, S. C., Lacy, J. H., Townes, C. H., Aller, L. H., Geballe, T. R., & Baas, F. 1981, ApJ, 249, 592
Black, J. H., & van Dishoeck, E. F. 1987, ApJ, 322, 412
Bowen, I. S. 1947, PASP, 59, 196
Dayal, A., & Bieging, J. H. 1996, ApJ, 472, 703
Draine, B. T. 1989, in Infrared Spectroscopy in Astronomy, ed. B. H. Kaldeich (ESA SP-290) (Paris: ESA), 93
Galavís, M. E., Mendoza, C., & Zeippen, C. J. 1995, A&AS, 111, 347
Geballe, T. R., Burton, M. G., & Isaacman, R. 1991, MNRAS, 253, 75
Gillett, F. C., Merrill, K. M., & Stein, W. A. 1972, ApJ, 172, 367
Grandi, S. A. 1975, ApJ, 196, 465
———. 1976, ApJ, 206, 658
———. 1980, ApJ, 238, 10
Grevesse, N., & Anders, E. 1989, in AIP Conf. Proc. 183, Cosmic Abundances of Matter, ed. C. J. Waddington (New York: AIP), 1
Grevesse, N., Noels, A., & Sauval, A. J. 1996, in ASP Conf. Ser. 99, Cosmic Abundances, ed. S. S. Holt & G. Sonneborn (San Francisco: ASP), 117
Gussie, G. T., & Taylor, A. R. 1995, MNRAS, 273, 801
Hoffleit, D., & Jaschek, C. 1982, The Bright Star Catalogue (4th rev. ed.; New Haven: Yale Univ. Obs.)
Hoffman, R. D., Woosley, S. E., Weaver, T. A., Rauscher, T., & Thielemann, F.-K. 1999, ApJ, 521, 735
Hora, J. L., Latter, W. B., & Deutsch, L. K. 1999, ApJS, 124, 195
Huggins, P. J., & Healy, A. P. 1989, ApJ, 346, 201
Isaacman, R. 1984, A&A, 130, 151
Kastner, J. H., Weintraub, D. A., Gatley, I., Merrill, K. M., & Probst, R. G. 1996, ApJ, 462, 777
Keenan, F. P., Aller, L. H., Bell, K. L., Hyung, S., McKenna, F. C., & Ramsbottom, C. A. 1996, MNRAS, 281, 1073
Koornneef, J. 1983, A&A, 128, 84
Kurucz, R. L. 1991, in Precision Photometry: Astrophysics of the Galaxy, ed. A. G. D. Philip, A. R. Upgren, & K. A. Janes (Schenectady: L. Davis), 27
Lowe, R. P., Moorhead, J. M., & Wehlau, W. H. 1979, ApJ, 228, 191
Martini, P., Sellgren, K., & Hora, J. L. 1997, ApJ, 484, 296
McKenna, F. C., Keenan, F. P., Kaler, J. B., Wickstead, A. W., Bell, K. L., & Aggarwal, K. M. 1996, PASP, 108, 610
Mendoza, C. 1983, in IAU Symp. 103, Planetary Nebulae, ed. D. R. Flower (Dordrecht: Reidel), 143
Phillips, J. P. 1998, A&A, 340, 527
Rudy, R. J., Cohen, R. D., Rossano, G. S., Erwin, P., Puetter, R. C., & Lynch, D. K. 1991a, ApJ, 380, 151
Rudy, R. J., Erwin, P., Rossano, G. S., & Puetter, R. C. 1992, ApJ, 384, 536
Rudy, R. J., Puetter, R. C., & Mazuk, S. 1998, AJ, 118, 666
Rudy, R. J., Rossano, G. S., Erwin, P., & Puetter, R. C. 1991b, ApJ, 368, 468
Rudy, R. J., Rossano, G. S., Erwin, P., Puetter, R. C., & Feibelman, W. A. 1993, AJ, 105, 1002

Rudy, R. J., Rossano, G. S., & Puetter, R. C. 1989, ApJ, 346, 799
Schlegel, D. J., Finkbeiner, D. P., & Davis, M. 1998, ApJ, 500, 525
Schwartz, R. D., Cohen, M., & Williams, P. M. 1987, ApJ, 322, 403
Smith, H. A., Larson, H. P., & Fink, U. 1981, ApJ, 244, 835
Smits, D. P. 1991, MNRAS, 251, 316
Stanghellini, L., & Kaler, J. B. 1989, ApJ, 343, 811
Sternberg, A., & Neufeld, D. A. 1999, ApJ, 516, 371
Storey, P. J., & Hummer, D. G. 1995, MNRAS, 272, 41
Takayanagi, K., Sakimoto, K., & Onda, K. 1987, ApJ, 318, L81
Tanaka, M., Hasegawa, T., Hayashi, S. S., Brand, W. J. L., & Gatley, I. 1989, ApJ, 336, 207
Taylor, A. R., Gussie, G. T., & Pottasch, S. R. 1990, ApJ, 351, 515
Treffers, R. R., Fink, U., Larson, H. P., & Gautier, T. N., III. 1976, ApJ, 209, 793
Volk, K., & Cohen, M. 1990, AJ, 100, 485
Woosley, S. E., Fowler, W. A., Holmes, J. A., & Zimmerman, B. A. 1978, At. Data Nucl. Data Tables, 22, 371
Zhang, C. Y., & Kwok, S. 1992, ApJ, 385, 255 (ZK)
Zuckerman, B., & Aller, L. H. 1986, ApJ, 301, 772